Spin-orbit interaction enhancement in permalloy thin films by Pt doping

A. Hrabec, F. J. T. Gonçalves, C. S. Spencer, E. Arenholz, A. T. N'Diaye, R. L. Stamps, and Christopher H. Marrows

Phys. Rev. B **93**, 014432 — Published 21 January 2016

DOI: 10.1103/PhysRevB.93.014432

Spin-orbit interaction enhancement in Permalloy thin films by Pt-doping

A. Hrabec,[1,*] F. J. T. Gonçalves,[2] C. S. Spencer,[1] E. Arenholz,[3]
A. T. N'Diaye,[3] R. L. Stamps,[2] and Christopher H. Marrows[1,†]

[1] *School of Physics and Astronomy, University of Leeds, Leeds LS2 9JT, United Kingdom*
[2] *SUPA, School of Physics and Astronomy, University of Glasgow, G12 8QQ, United Kingdom*
[3] *Advanced Light Source, Lawrence Berkeley National Laboratory, Berkeley, California 94720, USA*

(Dated: December 7, 2015)

The spin-orbit interaction is an inherent part of magnetism, which links up the independent world of spins to the atomic lattice, thus controlling many functional properties of magnetic materials. In the widely-used 3*d* transition metal ferromagnetic films, the spin-orbit interaction is relatively weak, due to low atomic number. Here we show that it is possible to enhance and tune the spin-orbit interaction by adding 5*d* platinum dopants into Permalloy ($Ni_{81}Fe_{19}$) thin films by a co-sputtering technique. This is achieved without significant changes of the magnetic properties, due to the vicinity of Pt to meeting the Stoner criterion for the ferromagnetic state. The spin-orbit interaction is investigated by means of transport measurements (the anisotropic magnetoresistance and anomalous Hall effect), ferromagnetic resonance measurements to determine the Gilbert damping, as well as by measuring the the x-ray magnetic circular dichroism at the L_3 and L_2 x-ray absorption edges to reveal the ratio of orbital to spin magnetic moments. It is shown that the effective spin-orbit interaction increases with Pt concentration within the 0-10 % Pt concentration range in a way that is consistent with theoretical expectations for all four measurements.

PACS numbers: 75.70.Tj; 75.76.+j; 75.50.-y

I. INTRODUCTION

The spin-orbit interaction (SOI) is the underlying effect for many phenomena in magnetism, since it connects two independent worlds: that of the orbital angular momentum **L**, which is closely connected to the atomic lattice, and the electron spin magnetic angular momentum **S**, a quantity that otherwise exists on its own in the world of quantum mechanics. The SOI is often expressed as $\xi \mathbf{S} \cdot \mathbf{L}$, where ξ is the SOI constant. Since the SOI is strongly influenced by the nuclei, large effects occur when a heavy element with a large nuclear charge, such as Pt or Au, is involved. Since the 3*d* ferromagnets–Fe, Co, Ni, and their alloys–are relatively light, the SOI is comparatively weak in these conventional ferromagnets. Therefore a combination of a heavy element with a ferromagnet is one of the possible ways to drive a stronger SOI within a conventional ferromagnet. For instance, the physics of thin magnetic films has recently attracted a lot of attention due to new emerging phenomena when a heavy metal is brought in contact with a thin ferromagnet. In such a way magnetic moments sitting at the surface of the ferromagnet experience the broken spatial symmetry and consequently give rise to new interfacial interactions which can have crucial impact on those surface states[1–4]. The other way to enhance the SOI in the ferromagnet is to dope it with a heavy element, as has been demonstrated in doped magnetic semiconductors[5]. Since the SOI affects a vast number of magnetic properties, may of which are important for various nanomagnetic or spintronic technologies, it would be convenient to tailor its strength and observe its impact on properties such as anisotropic magnetoresistance (AMR)[6], anomalous Hall effect (AHE)[7], magnetization damping phenomena[8,9] or different contributions to the torque acting on a magnetic domain wall by a field[10] or a spin-polarized current[11].

Permalloy (Py = $Ni_{81}Fe_{19}$) is a widely used material due to its unique properties combining a small magnetocrystalline anisotropy and a negligible magnetostriction constant. Besides these properties it has also high relative permeability, the property that initially attracted attention to it[12]. It has thus become an interesting material for many aspects of nanomagnetism and spintronics research. The effect of 3*d*, 4*d* and 5*d* transition metal doping of Py on the Gilbert damping has been systematically studied showing a relation to Hund's rules[13,14]. Here we report an investigation of the influence of Pt doping on the SOI of Py in the range of Pt concentrations up to 10%, where the magnetic properties of the ferromagnet are maintained. We have probed the SOI strength using magnetotransport (AMR and AHE), measurements of the Gilbert damping α through ferromagnetic linewidth measurements, and X-ray magnetic circular dichroism (XMCD), which have all provided consistent results. This cross-correlation of the different effects of changing the SOI strength gives a comprehensive overview of the interplay between the SOI strength and various observable properties. Thus, we have shown that the SOI can be controlled by the Pt concentration in Py in order to fine-tune functional properties.

II. EXPERIMENT

A. Thin film growth and characterization

The magnetic films were deposited by co-sputtering using Py and $Py_{90}Pt_{10}$ targets at base pressure of 10^{-8} Torr

and Ar pressure of 5×10^{-3} Torr. The exact balance between the rates from the two targets determined the final overall Pt doping level in the film which is deduced from the stoichiometry of the targets. 20 nm thick films of Py, $Py_{97.5}Pt_{2.5}$, $Py_{95}Pt_5$, $Py_{92.5}Pt_{7.5}$ and $Py_{90}Pt_{10}$ compositions have been sputtered directly onto thermally oxidized silicon substrates. Because of the co-sputtering method, the relative uncertainties in the film stoichiometries are small. Deposition rates were about 1 Å/s and the film thicknesses were calibrated by low-angle x-ray reflectometry. The films are uncapped apart from the set of samples used for synchrotron measurements where a layer of Al (2 nm) was used to protect the surface. No magnetic field was applied during the deposition to minimize parasitic effects of uniaxial anisotropy in our experiments.

The magnetic properties were characterized with vibrating sample magnetometry (VSM) where the magnetization of Py $M_{\rm Py} = 660 \pm 20$ kA/m and of $Py_{90}Pt_{10}$ $M_{\rm PyPt} = 650 \pm 20$ kA/m, unchanged to within the uncertainty. The magnetisation of all the other films was the same to within this uncertainty. The inset of Fig. 1 shows a VSM data set of normalized magnetization $M_{\rm s}$ as a function of temperature T for various levels of Pt doping. All the curves are seen to be very similar. In order to obtain the exchange stiffness constant A, the experimental points are fitted using the Bloch law $M_{\rm s} = 1 - cT^{3/2}$ from which the exchange stiffness can be determined by using the formula $A = 4.22 \times 10^8 k_{\rm B}/c^{2/3}$. The results of doing so are shown in Fig. 1. The change of A is very small in comparison with previously reported suppression of A in Py doped with Gd[15] or V[16]. Such a small variation of A can be attributed to the fact that Pt tends to be easily polarized by the surrounding ferromagnetic atoms, since it is very close to satisfying the Stoner criterion as a pure element, and therefore it does not significantly affect the ferromagnetic state[17].

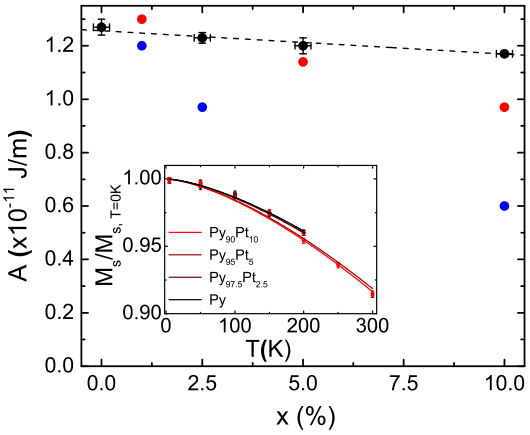

FIG. 1. Exchange stiffness A as a function of x in Py_xPt_{1-x} 20 nm thick films. Blue and red data points correspond to results for Gd and V doped Py which were extracted from Ref. 15 and Ref. 16, respectively. The black dashed line corresponds to a linear fit to the data for Pt. The inset shows temperature dependent normalized magnetization for different films with corresponding fits of the $T^{3/2}$ Bloch law.

B. Magnetotransport

To determine the impact of Pt doping on the SOI, two types of magnetotransport measurements, directly connected to the SOI, were carried out: AHE and AMR. In order to measure the AHE, a set of films was deposited with a Hall bar structure, with the cross feature of size 50 μm $\times$ 50 μm, using a shadow mask deposition technique. The Hall resistivity $\rho_{\rm AH}$ was measured at room temperature by a standard four-probe method with the field normal to the sample plane. The room temperature Hall hysteresis loops are shown in Fig. 2(a).

The transverse resistivity ρ_{xy} is described by an empirical formula

$$\rho_{xy} = R_{\rm o} B + R_{\rm s} M_z \qquad (1)$$

where $R_{\rm o}$ is the ordinary Hall resistivity coefficient and $R_{\rm s}$ is the anomalous Hall resistivity coefficient[7]. Unlike $R_{\rm s}$, the mechanism of ordinary Hall effect is well understood and $R_{\rm o}$ depends only on the inverse density of carriers, therefore it is found to be small in metals. The anomalous Hall resistivity, $\rho^{\rm A}_{xy} = R_{\rm s} M_z$ was obtained by the usual method of extrapolating the high field Hall resistivity data back to zero field. The dependence of $\rho^{\rm A}_{xy}$ on x is shown in Fig. 2(b), where a linear dependence on x is clearly evident, with ξ roughly quadrupling when 10 % Pt is added to Py.

It is now generally believed that the AHE comprises three contributions, each with different underlying physics: the intrinsic mechanism, which arises due to the SOI causing Berry curvature of the electron bands; and two extrinsic contributions arising from the skew and side-jump scattering mechanisms[7]. The knowledge of how the longitudinal σ_{xx} and anomalous Hall σ^A_{xy} conductivities scale with each other allows some distinction between these mechanisms. Here, σ^A_{xy} increases as the temperature is varied for $x = 10$ % in a manner that is rather linear in x, as can be seen from the data in the inset of Fig. 2(b), which is consistent with the skew scattering mechanism but not the intrinsic or side-jump scattering.

Considering the room temperature data across the series of samples with different x, we find that σ_{xx} lies in the range $(2.3\pm0.2)\times10^4$ $(\Omega{\rm cm})^{-1}$ for them all, with little discernible systematic dependence on x. This is reasonable since in a sputtered films of a transition metal solid solution like Py there is already strong disorder and some additional Pt impurity atoms will hardly affect the overall scattering rate. It is therefore reasonable to consider that the stronger SOI induced by the presence of the Pt gives rise to skew scattering that has a larger 'skew angle', albeit at a similar overall scattering rate, leading to a higher anomalous Hall conductivity, suggesting the

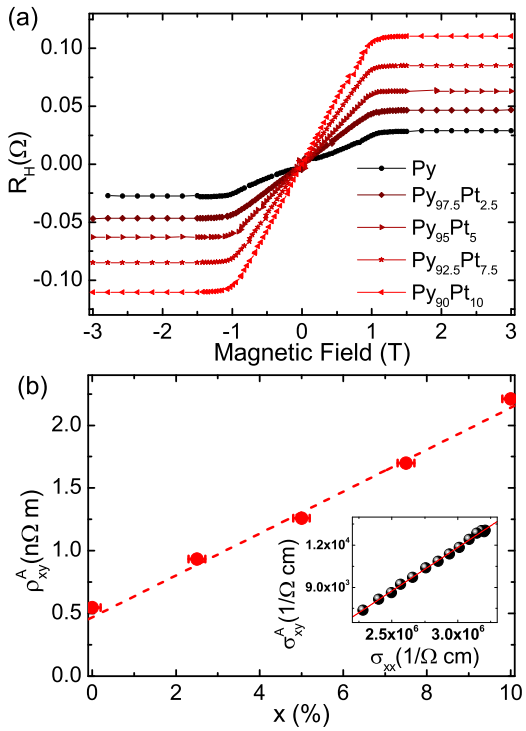

FIG. 2. Anomalous Hall effect at room temperature. (a) Hall resistance $R_{\rm H}$ at room temperature in films with various Pt content as a function of out-of-plane magnetic field. (b) Anomalous Hall resistivity as a function of Pt content. The red dashed curve represents a linear fit to the data. The error bars are smaller than the data points. The inset shows the dependence of the anomalous Hall conductivity on the longitudinal conductivity in the case of $x = 10$ %.

proportionality $\sigma^{\rm A}_{xy} \propto \xi$, where ξ rises linearly in x as the introduction of Pt increases the overall SOI strength from the low initial level found in undoped Py. While this proportionality is certainly not to be expected in general,[18] if the SOI strength is rather small, then the spin-conserving transitions will dominate and the scaling of $\rho^{\rm A}_{xy}$ with the SOI strength ξ should be dominated by a linear term[19].

Turning to the AMR, this effect is driven mainly by the probability of *s-d* scattering, leading to a dependence of the resistivity on the relative orientation of the magnetization M and electric current I. It is defined as $(R_\perp - R_\parallel)/R\perp$, where $R_\perp$ and $R_\parallel$ are the resistances in $\mathbf{I}\|\mathbf{M}$ and $\mathbf{I}\perp\mathbf{M}$ configurations, respectively. AMR data for undoped Py is shown in the inset of Fig. 3. The value of 2.6 % compares well to other data on thin Py films[20]. The AMR dependence on the Pt content x was extracted from a series of such measurements across the set of samples, and is displayed in Fig. 3, showing that the AMR increases with increasing Pt content up to 5.8 % for $Py_{90}Pt_{10}$. This enhancement easily reaches the Py bulk value and compares well with the large AMR ratios of 6-7 % in $Co_{70}Fe_{30}$[6]. It does not appear to be linear in x.

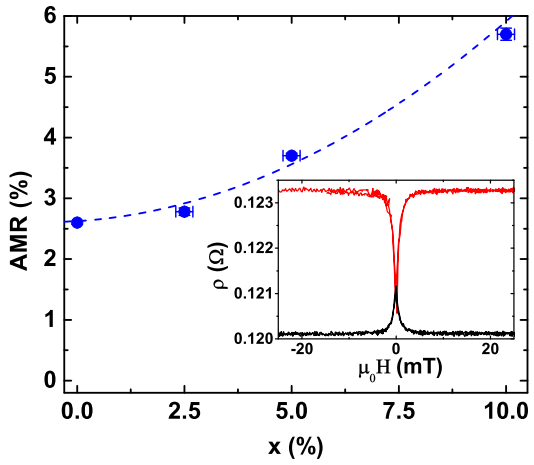

FIG. 3. AMR as a function of Pt content. The blue curve represents a fit to the AMR data as described in the text. The inset shows an example of AMR measurements in $\mathbf{I}\|\mathbf{M}$ (red) and $\mathbf{I}\perp\mathbf{M}$ (black) configurations for an undoped Py film.

Campbell *et al.* proposed a model for the AMR mechanism in strong ferromagnets that works well for Ni-based alloys[21]. The maximum AMR is of the order of $\frac{3}{4}\left(\xi/E_{\rm ex}\right)^2(\zeta - 1)$, where $E_{\rm ex}$ is the exchange splitting and the parameter ζ is derived from the residual resistivity, which depends on the type of impurity and is independent of impurity concentration and temperatures well below $T_{\rm c}$. The AMR therefore scales quadratically with the SOI. Based on the arguments given above with regard to the AHE, we assume the relationship

$$\xi(x) = \xi_{\rm Py} + kx, \tag{2}$$

where $\xi_{\rm Py}$ is the SOI of pure Py, and k is a scaling constant. The blue curve in Fig. 3 represents a fit of the square of Eq. 2 to the data, motivated by the fact that the variation in $E_{\rm ex}$ with x is likely to be very small, given the small variation in A shown in Fig. 1. The good agreement between the fit and the data demonstrates that the increase of the AMR is consistent with such a model.

C. Ferromagnetic Resonance

The SOI is also closely linked to the magnetization dynamics, since it gives rise to dissipation and damping. Once the magnetization $\mathbf{M}$ is excited from the equilibrium state, its motion is described by the Landau-Lifshitz-Gilbert equation:

$$\frac{{\rm d}\mathbf{M}}{{\rm d}t} = -\gamma\mathbf{M}\times\mathbf{B}_{\rm eff} + \frac{\alpha}{\mathbf{M}}\left(\mathbf{M}\times\frac{{\rm d}\mathbf{M}}{{\rm d}t}\right), \tag{3}$$

where $\gamma = |g\mu_{\rm B}/\hbar|$ is the gyromagnetic ratio, $\hbar$ is the reduced Planck constant, and $\mu_{\rm B}$ is the Bohr magneton. Beside the first precessional term expressing an infinite magnetization rotation around the effective field $\mathbf{B}_{\rm eff}$, the

equation also includes a second term representing energy dissipation, allowing the magnetization to relax into the direction of the effective magnetic field. This term is purely phenomenological and it controls the rate at which the magnetization reaches its equilibrium. Its strength is given by the Gilbert damping parameter α. Because this process does not conserve the spin there is an obvious connection to the SOI. Although this phenomenon is at the heart the magnetization dynamics, its exact mechanism is not fully understood. A commonly cited theory is the Kamberský Fermi-surface breathing model, in which α is calculated based on the SOI-induced spin-flip scattering rate as well as on the ordinary scattering[22]

$$\alpha \sim \frac{\mu_B D(E_F)(\Delta g)^2}{\tau \gamma M_s}, \tag{4}$$

where τ is the electron momentum scattering time, $D(E_F)$ is the density of states at the Fermi level, and the change in g-factor is expressed as $\Delta g = g - 2$.

The Gilbert damping can be experimentally measured for example by the time resolved magneto-optical Kerr effect technique[23], or by domain wall velocity measurements[24], but most commonly by measuring linewidths in ferromagnetic resonance (FMR) although significant discrepancies can arise due to film inhomogeneities[25]. To determine α, we have employed a vector network analyser FMR method, where the resonance lineshape is measured through the relative variation of the forward transmission parameter S_{21} of a two-port microstrip circuit. This quantity is measured as a function of the frequency and external applied field. Examples of such absorption peaks for different frequencies are displayed in Fig. 4(a) for a Permalloy film. One can clearly see that these peaks broaden with the increasing frequency f in the expected manner. The damping α was obtained from fits of the expression

$$\Delta H = \Delta H_0 + \frac{4\pi\alpha}{\mu_0 \gamma} f \tag{5}$$

where ΔH is the absorption full width at half maximum (FWHM) and ΔH_0 is the inhomogeneous contribution to the linewidth[26]. The ΔH as a function of frequency for different $Py_{1-x}Pt_x$ films is shown in inset of Fig. 4(b) and the resulting α values are plotted as a function of Pt content x in Fig. 4(b). The damping increases from 0.0095 ± 0.0005 for pure Py up to 0.0141 ± 0.0002 for $Py_{90}Pt_{10}$. The relationship between α and x does not appear to be linear. The dashed line in represents a quadratic fit to the data, which will be discussed in more detail below.

D. X-ray Magnetic Circular Dichroism

In the light of the relationship between the damping constant and the g-factor in the Kamberský model (Eq. 4), it is desirable to gain information about the

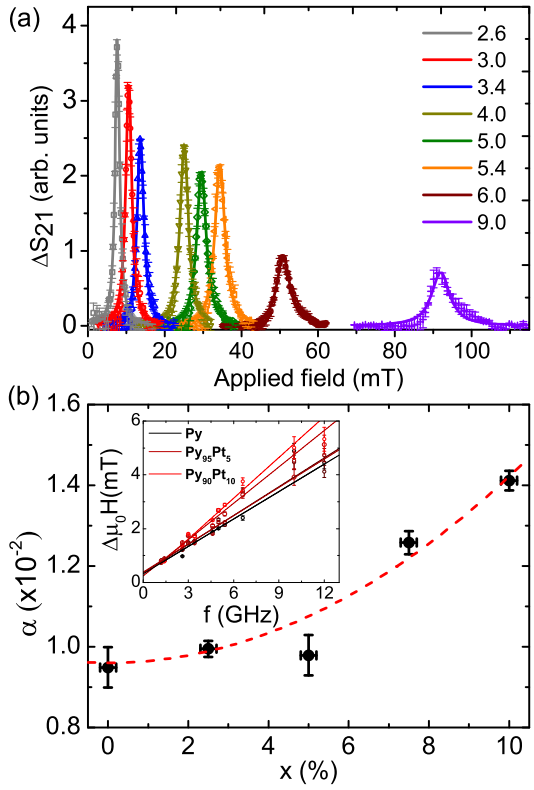

FIG. 4. Ferromagnetic resonance measurements. (a) Absorption ΔS_{21} for different frequencies given in GHz as a function of applied magnetic field, from which the FWHM ΔH can be obtained. (b) The inset depicts ΔH as a function of a fixed frequency for different Pt contents. The damping parameter α is calculated by using equation (5) and the results are displayed in the main plot of this panel. The red dashed curve represents a quadratic fit to the data.

g-factor in our films. In the case of $3d$ transition metals, the orbital magnetic moment is almost completely quenched by the surrounding crystal fields, and so the g-factor is very close to the free-electron value of 2. The deviation of the g-factor from the free-electron value is proportional to ξ/Δ, where Δ is the ground state-first excited state splitting of the corresponding $3d$ ion, and therefore reflects the strength of the SOI. For small orbital contributions it can be expressed as[27]

$$g = 2\left(\frac{\mu_L}{\mu_S} + 1\right) \tag{6}$$

where μ_L and μ_S are the orbital and spin magnetic moment respectively. This formula can be extended to alloys and compounds[27], and the effective g-factor g_{eff} in the case of Py reads

$$g_{eff} = (0.81M_{Ni} + 0.19M_{Fe}) \Big/ \left(\frac{0.81M_{Ni}}{g_{Ni}(x)} + \frac{0.19M_{Fe}}{g_{Fe}(x)}\right) \tag{7}$$

where $g_{Ni}(x)$ and $g_{Fe}(x)$ are the Pt concentration dependent g-factors of Ni and Fe obtained by Eq. 6 and

$M_{\mathrm{Ni}} = 0.69\mu_{\mathrm{B}}$ and $M_{\mathrm{Fe}} = 2.28\mu_{\mathrm{B}}$ are the magnetizations per atom of Ni and Fe respectively[28]. In this model we suppose that the magnetizations of Fe and Ni sublattices remain unchanged as Pt is introduced. This assumption is based on the total insensitivity of the magnetization of $\mathrm{Py}_{1-x}\mathrm{Pt}_x$ to the value of x reported above.

It is possible to straightforwardly measure the ratio $\mu_{\mathrm{L}}/\mu_{\mathrm{S}}$ using the X-ray magnetic circular dichroism (XMCD) technique. We did so here with measurements that were performed at beamline BL6.3.1.1 at the Advanced Light Source. Due to the surface sensitivity of this technique, the magnetic layers for this part of the study were capped by 2 nm of Al, which forms a self-limiting oxide. The total electron yield intensities μ_+ and μ_- around the L_3 and L_2 edges for Fe (690 eV-760 eV) and Ni (820 eV-920 eV) were measured in 30° grazing incidence with the sample saturated in a positive or negative magnetic field. The x-ray absorption spectroscopy (XAS) and XMCD ($\mu_+ - \mu_-$) spectra that were measured are plotted in Fig. 5(a).

By using the XMCD sum rules[29], these spectra were used to calculate the ratio of orbital magnetic moment μ_L and the spin magnetic moment μ_S for both Fe and Ni according to the formula

$$\frac{\mu_{\mathrm{L}}}{\mu_{\mathrm{S}}} = \frac{2q}{9p - 6q}, \tag{8}$$

where p is the integral under the L_3 XMCD peak and q is the integral under the L_2 peak. The results are plotted as a function of x in Fig. 5(b). The $\mu_{\mathrm{L}}/\mu_{\mathrm{S}}$ values measured in pure Permalloy correspond to the data measured previously[30]. The behavior of the $\mu_{\mathrm{L}}/\mu_{\mathrm{S}}$ ratios for Fe and Ni as Pt is added are rather different though. The ratio for Fe rises smoothly and linearly, whilst that for Ni fluctuates around a constant value without any discernible pattern. The reason for this is not clear at present, and we hope that this intriguing result will stimulate future studies in this area, both experimental and theoretical.

Inserting these values into Eq. 6, the g-factors for the Ni and Fe magnetic sublattices were obtained. These were combined according to Eq. 7 to give the effective g-factor g_{eff}, and the results are plotted in Fig. 5(c) as a function of Pt doping x. One can see that g_{eff} factor increases with the Pt concentration, signaling the SOI enhancement. This linear trend of $\mu_{\mathrm{L}}/\mu_{\mathrm{S}}$ with x–partly masked by the fluctuations arising from the Ni results–justifies, through the Kamberský model (Eq. 4), the quadratic-in-x fit to the α data in Fig. 4(b). The fact that g_{eff} would show a much smoother trend with x if we neglected the Ni and only treated the clear variation in $\mu_{\mathrm{L}}/\mu_{\mathrm{S}}$ for the Fe suggests that a more sophisticated theoretical treatment, perhaps based on first principles calculations, could yield a better formula to use that that in Eq. 7 to treat cases such as this. The g-factor in Fig. 5(c) obtained by the XMCD technique shows a good agreement with Δg obtained from the FMR data calculated by Eq. 4.

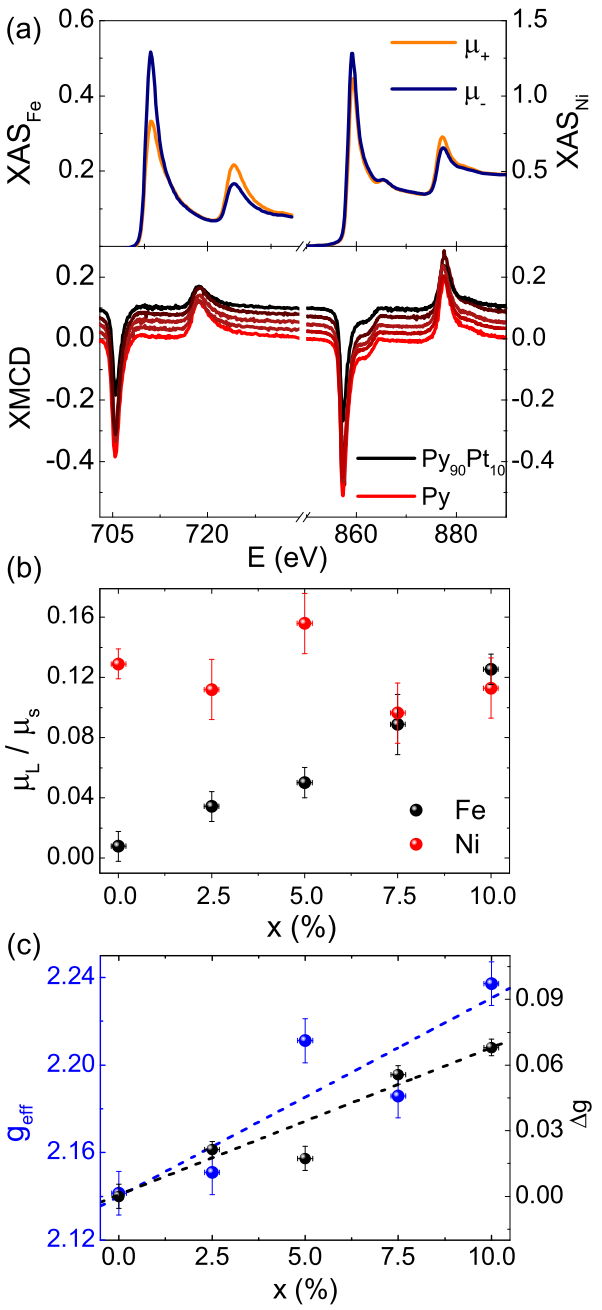

FIG. 5. (a) XAS spectra for right μ_+ and left μ_- circularly polarized x-rays in pure Py film. The XMCD contrast is obtained by subtracting these two intensities. The XMCD data is mutually offset for clarity. (b) Ratio of spin and orbital magnetic moments and as a function of Pt doping extracted from Fe (black) and Ni (red) absorption edges. (c) Calculated g_{eff} as a function of Pt concentration. The blue dashed line corresponds to linear fit to the data. Δg is obtained from FMR data by using Eq. 4. The black dashed line corresponds to linear fit of the data.

III. CONCLUSIONS

In our experimental work we show that heavy element doping of Permalloy with Pt can lead to a significant enhancement of the SOI. This was proved by a series of transport measurements, element specific XMCD observations and by the magnetization dynamics behaviour, which showed an enhancement of the Gilbert damping. The spin-orbit interaction ξ increases linearly with Pt concentration x within the 0-10 % Pt concentration range in way that is consistent with theoretical expectations across all four measurements. This gives a comprehensive overview of the way in which changes in the SOI strength affects the interplay of different observable magnetic properties, many of which are of technological importance.

ACKNOWLEDGMENTS

This work was supported by the EPSRC (grant numbers EP/I011668/1, EP/M024423/1, EP/I013520/1 and EP/J000337/1). The Advanced Light Source is supported by the Director, Office of Science, Office of Basic Energy Sciences, of the U.S. Department of Energy under Contract No. DE-AC02-05CH11231. We would like to thank G. Tatara for the discussions that led to the suggestion for these experiments, and Y. Mokrousov for enlightening discussions about the scaling of the anomalous Hall effect.

* Present address: Laboratoire de Physique des Solides, CNRS, Universités Paris-Sud et Paris-Saclay, 91405 Orsay Cedex, France
† Email: c.h.marrows@leeds.ac.uk

[1] O Krupin, G Bihlmayer, K Starke, Serguei Gorovikov, JE Prieto, K Döbrich, S Blügel, and G Kaindl, "Rashba effect at magnetic metal surfaces," Phys. Rev. B **71**, 201403 (2005).
[2] M. I. Miron, G. Gaudin, S. Auffret, B. Rodmacq, A. Schuhl, S. Pizzini, J. Vogel, and P. Gambardella, "Current-driven spin torque induced by the Rashba effect in a ferromagnetic metal layer," Nature Mat. **9**, 230 (2010).
[3] G. Chen, T. Ma, A. T. N'Diaye, H. Kwon, C. Won, Y. Wu, and A. K. Schmid, "Tailoring the chirality of magnetic domain walls by interface engineering," Nat. Commun. **4**, 2671 (2013).
[4] A. Fert, "Magnetic and transport properties of metallic multilayers," in *Materials Science Forum*, Vol. 59 (Trans. Tech. Publ., 1991) p. 439.
[5] T. Jungwirth, Q. Niu, and A. H. MacDonald, "Anomalous Hall effect in ferromagnetic semiconductors," Phys. Rev. Lett. **88**, 207208 (2002).
[6] T. R. McGuire and R. I. Potter, "Anisotropic magnetoresistance in ferromagnetic 3*d* alloys," IEEE Trans. Magn. **11**, 1081 (1975).
[7] N. Nagaosa, J. Sinova, S. Onoda, A. H. MacDonald, and N. P. Ong, "Anomalous Hall effect," Rev. Mod. Phys. **82**, 1539 (2010).
[8] M. C. Hickey and J. S. Moodera, "Origin of intrinsic Gilbert damping," Phys. Rev. Lett. **102**, 137601 (2009).
[9] T. L. Gilbert, "A phenomenological theory of damping in ferromagnetic materials," IEEE Trans. Magn. **40**, 3443 (2004).
[10] T. A. Moore, P. Möhrke, L. Heyne, A. Kaldun, M. Kläui, D. Backes, J. Rhensius, L. Heyderman, J.-U. Thiele, G. Woltersdorf, A. F. Fraile Rodríguez, F. Nolting, Tevfik O. Menteş, M. Niño, A. Locatelli, A. Potenza, H. Marchetto, S. Cavill, and S. S. Dhesi, "Magnetic-field-induced domain-wall motion in permalloy nanowires with modified Gilbert damping," Phys. Rev. B **82**, 094445 (2010).
[11] A. Thiaville, Y. Nakatani, J. Miltat, and Y. Suzuki, "Micromagnetic understanding of current-driven domain wall motion in patterned nanowires," Europhys. Lett. **69**, 990 (2005).
[12] H. D. Arnold and G. W. Elmen, "Permalloy, a new magnetic material of very high permeability," Bell System Tech. J. **2**, 101 (1923).
[13] J. O. Rantschler, R. D. McMichael, A. Castillo, A. J. Shapiro, W. F. Egelhoff, B. B. Maranville, D. Pulugurtha, A. P. Chen, and L. M. Connors, "Effect of 3*d*, 4*d*, and 5*d* transition metal doping on damping in permalloy thin films," J. Appl. Phys. **101**, 033911 (2007).
[14] S. Mizukami, A. Sakuma, A. Sugihara, T. Kubota, Y. Kondo, H. Tsuchiura, and T. Miyazaki, "Influence of Pt doping on Gilbert damping in permalloy films and comparison with the perpendicularly magnetized alloy films," Jpn. J. Appl. Phys **50**, 103003 (2011).
[15] S. Lepadatu, J.S. Claydon, C.J. Kinane, S. Langridge, S.S. Dhesi, and C.H. Marrows, "Tuning of current-induced domain wall resonance frequency using Gd doping," Appl. Phys. Lett. **97**, 072507 (2010).
[16] S. Lepadatu, J.S. Claydon, C.J. Kinane, T.R. Charlton, S. Langridge, A Potenza, S. S. Dhesi, P.S. Keatley, R.J. Hicken, and B.J. Hickey, "Domain-wall pinning, nonadiabatic spin-transfer torque, and spin-current polarization in permalloy wires doped with vanadium," Phys. Rev. B **81**, 020413 (2010).
[17] S.-Y. Huang, X. Fan, D. Qu, Y. P. Chen, W. G. Wang, J. Wu, T. Y. Chen, J. Q. Xiao, and C. L. Chien, "Transport magnetic proximity effects in platinum," Phys. Rev. Lett. **109**, 107204 (2012).
[18] Y. Yao, L. Kleinman, A. MacDonald, J. Sinova, T. Jungwirth, D.-S. Wang, E. Wang, and Q. Niu, "First principles calculation of anomalous Hall conductivity in ferromagnetic bcc Fe," Phys. Rev. Lett. **92**, 037204 (2004).
[19] Y. Mokrousov, H. Zhang, F. Freimuth, B. Zimmermann, N. H. Long, J. Weischenberg, I. Souza, P. Mavropoulos, and S. Blügel, "Anisotropy of spin relaxation and transverse transport in metals," J. Phys.: Cond. Matt. **25**, 163201 (2013).
[20] T. G. S. M. Rijks, S. K. J. Lenczowski, R. Coehoorn, and W. J. M. De Jonge, "In-plane and out-of-plane anisotropic

magnetoresistance in $Ni_{80}Fe_{20}$ thin films," Phys. Rev. B **56**, 362 (1997).

[21] I. A. Campbell, A. Fert, and O. Jaoul, "The spontaneous resistivity anisotropy in Ni-based alloys," J. Phys. C **3**, S95 (1970).

[22] V Kamberskỳ, "On the Landau-Lifshitz relaxation in ferromagnetic metals," Can. J. Phys. **48**, 2906 (1970).

[23] T. Gerrits, H. A. M. Van Den Berg, J. Hohlfeld, L. Bär, and T. Rasing, "Ultrafast precessional magnetization reversal by picosecond magnetic field pulse shaping," Nature (London) **418**, 509 (2002).

[24] A. Thiaville, Y. Nakatani, J. Miltat, and N. Vernier, "Domain wall motion by spin-polarized current: a micromagnetic study," J. Appl. Phys. **95**, 7049 (2004).

[25] T. Weindler, H. G. Bauer, R. Islinger, B. Boehm, J.-Y. Chauleau, and C. H. Back, "Magnetic damping: Domain wall dynamics versus local ferromagnetic resonance," Phys. Rev. Lett. **113**, 237204 (2014).

[26] J.-M. Beaujour, D. Ravelosona, I. Tudosa, E. E. Fullerton, and A. D. Kent, "Ferromagnetic resonance linewidth in ultrathin films with perpendicular magnetic anisotropy," Phys. Rev. B **80**, 180415 (2009).

[27] A. J. P. Meyer and G. Asch, "Experimental g' and g values of Fe, Co, Ni, and their alloys," J. Appl. Phys. **32**, S330 (1961).

[28] Etienne du Tremolet De Lacheisserie, Damien Gignoux, and Michel Schlenker, *Magnetism: II-Materials and Applications* (Springer Science & Business Media, 2012).

[29] C. T. Chen, Y. U. Idzerda, H.-J. Lin, N. V. Smith, G. Meigs, E. Chaban, G. H. Ho, E. Pellegrin, and F. Sette, "Experimental confirmation of the X-ray magnetic circular dichroism sum rules for iron and cobalt," Phys. Rev. Lett. **75**, 152 (1995).

[30] B. Glaubitz, S. Buschhorn, F. Brüssing, R. Abrudan, and H. Zabel, "Development of magnetic moments in $Fe_{1-x}Ni_x$-alloys," J. Phys.: Cond. Matt. **23**, 254210 (2011).